A two scale nonlinear fractal sea surface model in a one dimensional deep sea*

Xie Tao(谢 涛)[a)b)†], Zou Guang-Hui(邹光辉)[a)],
William Perrie[b)], Kuang Hai-Lan(旷海兰)[a)], and Chen Wei(陈 伟)[a)]

[a)] School of Information Engineering of Wuhan University of Technology, Wuhan 430070, China
[b)] Fisheries and Oceans Canada, Bedford Institute of Oceanography, B2Y 4A2, Dartmouth, NS, Canada

(Received 17 July 2009; revised manuscript received 26 October 2009)

Using the theory of nonlinear interactions between long and short waves, a nonlinear fractal sea surface model is presented for a one dimensional deep sea. Numerical simulation results show that spectra intensity changes at different locations (in both the wave number domain and temporal-frequency domain), and the system obeys the energy conservation principle. Finally, a method to limit the fractal parameters is also presented to ensure that the model system does not become ill-posed.

Keywords: fractal sea surface models, nonlinear interaction, numerical method
PACC: 9210H, 9240C

1. Introduction

Although stochastic waves and periodic sine waves can be used to construct a rough sea surface,[1] in nature the sea surface is neither purely stochastic nor absolutely periodic. Thus, these models can not reliably show all of the characteristics of the sea surface. Fractal geometry[2] is a potentially important tool to characterise the sea surface because it can incorporate semi-stochastic and semi-periodic features.[3−5] In fact different linear fractal sea surface models have recently been used to simulate the sea surface[6−14] and land surfaces.[15]

Fractal sea surface models have been extensively applied to simulate electromagnetic (EM) scattering from a rough sea surface.[6−14] These models are limited to narrow band conditions. Although they can simulate the linear Gaussian sea surface, they cannot fully represent the real sea surface which is always full of nonlinear ocean waves. Moreover, nonlinear ocean waves involve nonlinear interactions between long and short waves, for example as discussed by Longuet-Higgins and Stewart[16] and many other researchers in recent decades. The discrepancies between EM echo signals scattering from a linear sea surface and those scattering from a nonlinear sea surface are large, as is evident when the EM echo from a rough sea surface is numerically calculated.[17] To reduce errors in estimates of EM echo signals, it is necessary to develop a nonlinear fractal sea surface model. In this letter, we present a relatively simple two-scale nonlinear fractal sea surface model for a one-dimensional (1D) deep sea.

2. Nonlinear fractal sea surface model in a 1D deep sea

A linear fractal Gaussian sea surface model was presented by Berizzi *et al.*[6−9] In the 1D case, the linear sea surface can be presented as:

$$f_{\text{linear}}(x,t) = \sum_{n=1}^{N} a_n \sin\psi_n, \tag{1}$$

where subscript $n(1 \le n \le N)$ denotes the nth sine wave component of the surface with amplitude $a_n = \sigma C b^{(s-2)(n-1)}$, phase $\psi_n = k_1 b^{n-1}(x + Vt) - \Omega_n t + \Phi_n$, wave number $k_n = k_1 b^{(n-1)}$ and frequency $\Omega_n = \sqrt{g k_n}$, sea surface current velocity is V. Here, $C = \sqrt{(2[1 - b^{2(s-2)}])/(1 - b^{2N(s-2)})}$, and b is a constant which relates to the auto-correlation function,[8] s is fractal dimension $(1 < s < 2)$, σ is the variance of the linear sea surface, and g is the gravitational accel-

*Project supported by Chinese National High Technology Research and Development (863) Program (Grant No. 2007AA12Z170), National Natural Science Foundation of China (Grant No. 40706058), Wuhan Youth Science and Technology Chen Guang Program (Grant No. 200850731388) and the wind and waves component of the Canadian Space Agency GRIP project entitled 'Building Satellite Data into Fisheries and Oceans Operational Systems'.
†Corresponding author. E-mail: xtplqk@whut.edu.cn
© 2010 Chinese Physical Society and IOP Publishing Ltd

eration. Initial phases Φ_n are uniformly distributed in $[-\pi, \pi]$. The mean value of $f_{\rm linear}(x,t)$ is zero.

In order to construct a relatively simple nonlinear fractal sea surface model, we apply the two-scale method of Longuet-Higgins and Stewart[16] to the linear sea surface model. One can divide the wave components into two groups, the long waves and the short waves. The separation criterion for these two groups is provided by the critical value $n_{\rm c} = N_0$; wave components satisfying $n \leq N_0$ belong to the long waves group, otherwise they are short waves. Here, N_0 is determined by the relation:

$$b^{(N_0+1)} - b^{(N_0)} \geq 10, \tag{2}$$

which suggests that $k_{N_0+1} \gg k_{N_0}$, and thus the nonlinear interaction relations for long and short waves of Longuet-Higgins and Stewart[16] can be applied. These nonlinear interactions are defined as:

$$\begin{aligned} f_{ls}(x,t) = & \left(a_l \sin\psi_l - \frac{1}{2}a_l^2 k_l \sin(2\psi_l)\right) + \left(a_s \sin\psi_s - \frac{1}{2}a_s^2 k_s \sin(2\psi_s)\right) \\ & - a_l a_s \left(k_s \cos\psi_l \cos\psi_s - k_l \sin\psi_l \sin\psi_s\right), \end{aligned} \tag{3}$$

where subscripts l and s denote long and short waves, respectively.

One can obtain the fractal ocean wave components of the sea surface, by considering the nonlinear interactions between each long and short waves. To begin with, the nonlinear sea surface elevation of the primary or base wave (with the longest wavelength denoted with subscript 1) nonlinearly interacts with the N_0+1st wave, the N_0+2nd ..., and the Nth short waves according to the following relations:

$$\begin{aligned} f_{(1,N_0+1)} = & \left(a_1 \sin\psi_1 - \frac{1}{2}a_1^2 k_1 \sin(2\psi_1)\right) + \left(a_{N_0+1} \sin\psi_{N_0+1} - \frac{1}{2}a_{N_0+1}^2 k_{N_0+1} \sin(2\psi_{N_0+1})\right) \\ & - a_1 a_{N_0+1} \left(k_{N_0+1} \cos\psi_1 \cos\psi_{N_0+1} - k_1 \sin\psi_1 \sin\psi_{N_0+1}\right), \end{aligned} \tag{4}$$

$$\begin{aligned} f_{(1,N_0+2)} = & \left(a_1 \sin\psi_1 - \frac{1}{2}a_1^2 k_1 \sin(2\psi_1)\right) + \left(a_{N_0+2} \sin\psi_{N_0+2} - \frac{1}{2}a_{N_0+2}^2 k_{N_0+2} \sin(2\psi_{N_0+2})\right) \\ & - a_1 a_{N_0+2} \left(k_{N_0+2} \cos\psi_1 \cos\psi_{N_0+2} - k_1 \sin\psi_1 \sin\psi_{N_0+2}\right), \end{aligned} \tag{5}$$

and

$$\begin{aligned} f_{(1,N)} = & \left(a_1 \sin\psi_1 - \frac{1}{2}a_1^2 k_1 \sin(2\psi_1)\right) + \left(a_N \sin\psi_N - \frac{1}{2}a_N^2 k_N \sin(2\psi_N)\right) \\ & - a_1 a_N \left(k_N \cos\psi_1 \cos\psi_N - k_1 \sin\psi_1 \sin\psi_N\right). \end{aligned} \tag{6}$$

Equations (7)–(9) represent the nonlinear interactions between the secondary long waves (denoted by subscript 2) and all the short waves,

$$\begin{aligned} f_{(2,N_0+1)} = & \left(a_2 \sin\psi_2 - \frac{1}{2}a_2^2 k_2 \sin(2\psi_2)\right) + \left(a_{N_0+1} \sin\psi_{N_0+1} - \frac{1}{2}a_{N_0+1}^2 k_{N_0+1} \sin(2\psi_{N_0+1})\right) \\ & - a_2 a_{N_0+1} \left(k_{N_0+1} \cos\psi_2 \cos\psi_{N_0+1} - k_2 \sin\psi_2 \sin\psi_{N_0+1}\right), \end{aligned} \tag{7}$$

$$\begin{aligned} f_{(2,N_0+2)} = & \left(a_2 \sin\psi_2 - \frac{1}{2}a_2^2 k_2 \sin(2\psi_2)\right) + \left(a_{N_0+2} \sin\psi_{N_0+2} - \frac{1}{2}a_{N_0+2}^2 k_{N_0+2} \sin(2\psi_{N_0+2})\right) \\ & - a_2 a_{N_0+2} \left(k_{N_0+2} \cos\psi_2 \cos\psi_{N_0+2} - k_2 \sin\psi_2 \sin\psi_{N_0+2}\right), \end{aligned} \tag{8}$$

and

$$\begin{aligned} f_{(2,N)} = & \left(a_2 \sin\psi_2 - \frac{1}{2}a_2^2 k_2 \sin(2\psi_2)\right) + \left(a_N \sin\psi_N - \frac{1}{2}a_N^2 k_N \sin(2\psi_N)\right) \\ & - a_2 a_N \left(k_N \cos\psi_2 \cos\psi_N - k_2 \sin\psi_2 \sin\psi_N\right). \end{aligned} \tag{9}$$

Similar expressions represent the nonlinear interactions between the shortest of the long waves and the short waves

$$f_{(N_0,N_0+1)} = \left(a_{N_0} \sin\psi_{N_0} - \frac{1}{2}a_{N_0}^2 k_{N_0} \sin 2(\psi_{N_0})\right) + \left(a_{N_0+1} \sin\psi_{N_0+1} - \frac{1}{2}a_{N_0+1}^2 k_{N_0+1} \sin(2\psi_{N_0+1})\right)$$

$$- a_{N_0} a_{N_0+1} \left(k_{N_0+1} \cos\psi_{N_0} \cos\psi_{N_0+1} - k_{N_0} \sin\psi_{N_0} \sin\psi_{N_0+1}\right), \tag{10}$$

$$f_{(N_0,N_0+2)} = \left(a_{N_0} \sin\psi_{N_0} - \frac{1}{2} a_{N_0}^2 k_{N_0} \sin(2\psi_{N_0})\right) + \left(a_{N_0+2} \sin\psi_{N_0+2} - \frac{1}{2} a_{N_0+2}^2 k_{N_0+2} \sin(2\psi_{N_0+2})\right)$$
$$- a_{N_0} a_{N_0+2} \left(k_{N_0+2} \cos\psi_{N_0} \cos\psi_{N_0+2} - k_{N_0} \sin\psi_{N_0} \sin\psi_{N_0+2}\right), \tag{11}$$

and

$$f_{(N_0,N)} = \left(a_{N_0} \sin\psi_{N_0} - \frac{1}{2} a_{N_0}^2 k_{N_0} \sin(2\psi_{N_0})\right) + \left(a_N \sin\psi_N - \frac{1}{2} a_N^2 k_N \sin(2\psi_N)\right)$$
$$- a_{N_0} a_N \left(k_N \cos\psi_{N_0} \cos\psi_N - k_{N_0} \sin\psi_{N_0} \sin\psi_N\right). \tag{12}$$

We add all the sea surface equations (4)–(12) together and obtain

$$\begin{aligned} F &= f_{(1,N_0+1)} + f_{(1,N_0+2)} + \ldots f_{(1,N)} + f_{(2,N_0+1)} + f_{(2,N_0+2)} + \ldots f_{(2,N)} + \ldots \\ &\quad + f_{(N_0,N_0+1)} + f_{(N_0,N_0+2)} + \ldots f_{(N_0,N)} \\ &= (N - N_0) \sum_{n=1}^{N} \left(a_n \sin\psi_n - \frac{1}{2} a_n^2 k_n \sin(2\psi_n)\right) \\ &\quad - \sum_{n=N_0+1}^{N} \sum_{m=1}^{N_0} a_n a_m \left[k_n \cos\psi_n \cos\psi_m - k_m \sin\psi_n \sin\psi_m\right]. \end{aligned} \tag{13}$$

Dividing by $N - N_0$, equation (13) becomes:

$$\begin{aligned} & f(x,t) \\ &= \frac{F}{N - N_0} \\ &= \frac{f_{(1,N_0+1)} + f_{(1,N_0+2)} + \ldots f_{(1,N)}}{(N - N_0)} + \frac{f_{(2,N_0+1)} + f_{(2,N_0+2)} + \ldots f_{(2,N)}}{(N - N_0)} + \ldots \\ &\quad + \frac{f_{(N_0,N_0+1)} + f_{(N_0,N_0+2)} + \ldots f_{(N_0,N)}}{(N - N_0)} \\ &= \sum_{n=1}^{N} \left(a_n \sin\psi_n - \frac{1}{2} a_n^2 k_n \sin(2\psi_n)\right) - \frac{1}{2(N - N_0)} \sum_{n=N_0+1}^{N} \sum_{m=1}^{N_0} a_n a_m \left[\begin{array}{l} (k_n + k_m) \cos(\psi_n + \psi_m) \\ +(k_n - k_m) \cos(\psi_n - \psi_m) \end{array}\right]. \end{aligned} \tag{14}$$

The first term of the right side of equation (14) is the linear fractal part of sea surface model. This is evident from equation (1), the linear fractal model developed by cited authors. Other terms of the right side of equation (14) can be regarded as constituting the nonlinear part of the proposed nonlinear fractal sea surface model, in a 1D deep sea.

3. Numerical results and discussion

In this section, nonlinear and linear fractal ocean waves are simulated with the following initial conditions $t = 0$: the longest wavelength of the spectra is c, with $\lambda_1 = 300$ m, $b = 2e/3$, fractal dimensions $s = 1.4$, $\sigma = 0.5$, the number of wave components is $N = 25$, and current velocity $V = 0.5$. According to equation (2), we infer that $N_0 = 12$.

To compare the nonlinear and linear fractal models, we present the numerical simulation results in the domain from $x = -300$ m to 300 m (twice the longest wavelength). The spatial variations in elevation of the linear and nonlinear fractal sea surface models are shown in Figs. 1(a) and 1(b), respectively. Figure 1(c) shows the elevation difference between the nonlinear and linear fractal models. It is evident that the nonlinear interactions essentially occur near the wave crest and trough locations in Fig. 1(c), which coincides with the results from Longuet-Higgins and Stewart.[16] Thus, we call these locations the nonlinear interactions areas. The numerical simulations suggest that the nonlinear fractal sea surface is rougher than the linear fractal sea surface, especially in the nonlinear interactions areas.

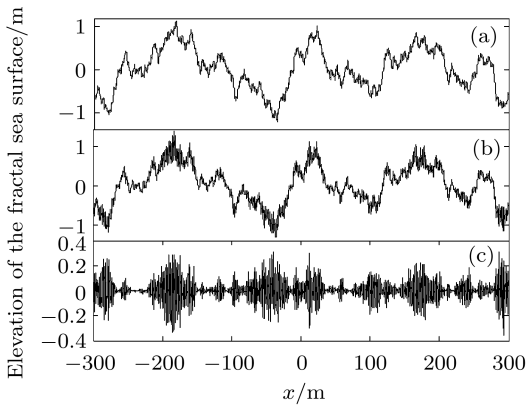


Fig. 1. Elevation of the fractal sea surface showing: (a) linear sea surface, (b) nonlinear sea surface, and (c) difference between linear minus nonlinear fractal sea surfaces. Units are m.

We use the same sea surface parameters as those of Johnson *et al.*,[18] and we compared the average normalised radar cross section (NRCS) for the nonlinear fractal sea surface model and that of the linear fractal sea surface within the nonlinear interactions area, with that of the so-called West model,[18,19] for different incidence angles (40° and 80°) and polarisation styles (VV/HH). The results are shown in Table 1. From Table 1, one can easily find that the NRCS is somewhat underestimated by the linear fractal sea surface model when calculating the electromagnetic wave scattering intensity from the sea surface for moderate to large incidence angles. This result is owing to the absence of contributions from nonlinear interactions between long and short waves.

Table 1. Average normalised radar cross sections of different models.

incidence angle/°	polarisation style	RCS/dB west model	RCS/dB nonlinear model	RCS/dB linear model
40	VV	–22.93	–22.99	–23.51
80	VV	–31.27	–31.53	–31.95
40	HH	–28.70	–28.92	–29.37
80	HH	–56.98	–57.08	–59.56

Fourier transforming the results in Fig. 1, we give the spectra intensities as a function of wave numbers in Fig. 2. To show the structural differences in the spectra intensities between linear and nonlinear models, we only show spectra intensities on the [0, 0.3] interval on the y-axis in Fig. 2.

Comparing the spectra intensities of the nonlinear and the linear models in Fig. 2, it is evident that several new spectra components are generated in the

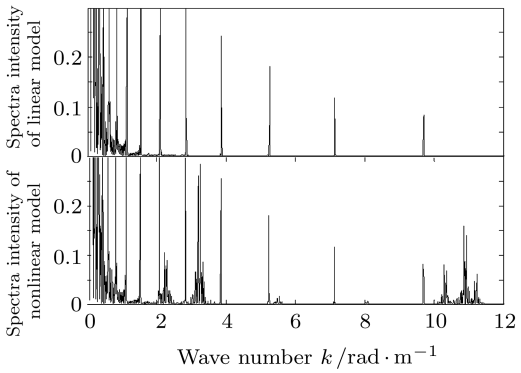


Fig. 2. Spectra intensity of the sea surface as a function of wavenumber: (upper panel) linear model, and (lower panel) nonlinear model.

former. For example, new spectra intensity components appear with different wave bands at $k = [2.00, 2.50]$, $[3.02, 3.50]$, $[5.40, 5.68]$, and $[10.08, 11.45]$ ... . Moreover, another difference between the nonlinear and linear fractal models is that the spectra intensities at some wavenumbers are increased, for example, at $k = 3.864$ rad/m, with spectra intensities of 0.244 in the linear model and 0.2557 in the nonlinear model, whereas in other instances spectra intensities are decreased; at $k = 7.138$ rad/m spectra intensities are 0.1182 in the linear fractal model and 0.1172 in the nonlinear model. These phenomena can be explained by energy conservation; an increase in spectra energy density at a given wave number must be linked to energy sinks at other wave numbers. Moreover, equation (14) implies that spectra intensities at wave numbers $k_n + k_m$ and $k_n - k_m$ should experience these changes.

Similar differences in spectra intensities of linear and nonlinear fractal models in the temporal-frequency domain are shown in Fig. 3. Changes in spectra intensity can again be explained by energy conservation, Eq. (14), in conjunction with the deep sea dispersion relationship $\Omega_n = \sqrt{gk_n}$.

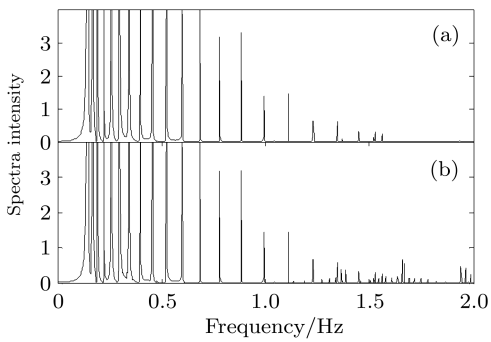


Fig. 3. As in Fig. 2, showing spectra intensity as a function of frequency for (upper plot) the linear model, and (lower plot) the nonlinear model.

It is well know that swell has dramatic effect on the energy spectra intensity of wind waves whose frequencies are higher than that of the swell. Donelan[20] depicted his finding from a tank experiment: 'The growth of the mechanical waves in response to the wind and the attenuation of the wind waves are apparent when both paddle and wind are exited together. It is noteworthy that the wind spectrum is not only dramatically reduced swell than without'. The phenomenon is caused by nonlinear interaction between swell and wind waves. Comparing spectra (see Figs. 2 and 3) of nonlinear fractal sea surface model with that of linear sea surface model, one can find that spectra of nonlinear fractal sea surface model are coincide with Donelan's result while linear fractal sea surface model without the case. To sum up, the simulating results of nonlinear fractal sea surface model is closer to real swell with wind sea states than those of linear fractal sea surface model.

Finally, the spectra intensity distribution with respect to wave number is calculated when N changes or λ_1 changes. Figures 4 and 5 presents the spectra intensity caused by the nonlinear interactions between long and short waves at high frequency areas of the domains. The bandwidth of these domains are affected mainly by the number of sine wave components N and the maximum wavelength λ_1. For example, the bandwidth becomes narrower when λ_1 increases in Fig. 4. Moreover, the bandwidth is broadened when N increases in Fig. 5.

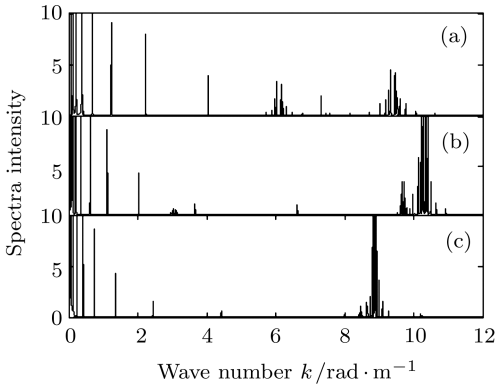


Fig. 4. Spectra intensity distribution with wave numbers at different wave length values of λ_1. (a) $N = 30$, $\lambda_1 = 150$; (b) $N = 30$, $\lambda_1 = 250$; (c) $N = 30$, $\lambda_1 = 350$.

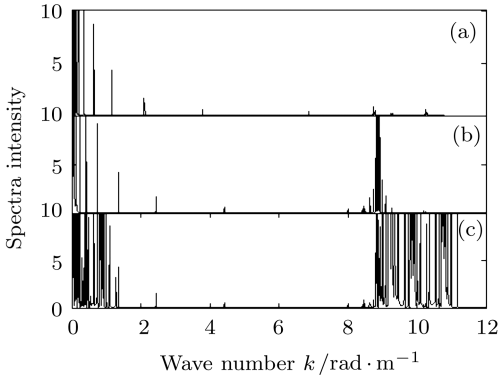


Fig. 5. Spectra intensity distribution with wave number at different numbers of sine wave components. (a) $N = 20$, $\lambda_1 = 200$; (b) $N = 30$, $\lambda_1 = 200$; (c) $N = 40$, $\lambda_1 = 200$.

4. Limitation of fractal parameters

Although fractal dimensions are limited to the range of $(1 \leq s \leq 2)$, N can become theoretically very large. However, numerical simulations will be ill-posed in the nonlinear fractal ocean model if N is larger than some critical value. According to Eq. (14), a possible factor causing ill-posed results is short wave steepness because the amplitude and wave number become large with increasing of n. The steepness (ε_n) of the nth wave component is the product of amplitude a_n and wave number k_n:

$$\varepsilon_n = a_n k_n = \frac{2\pi\sigma b^{(s-1)(n-1)}}{\lambda_1}\sqrt{\frac{2[1-b^{2(s-2)}]}{1-b^{2N(s-2)}}}. \quad (15)$$

Figure 6 shows that wave steepness is small when s and N are small. However, steepness increases sharply when $N > 40$, and when $s > 1.6$ at $N = 50$. When $t = 0$ and $x = 10$, Figure 6 shows that fractal dimensions s and number of sine components N can affect steepness, and that numerical simulations become ill-posed when $N > 40$ and $s > 1.6$.

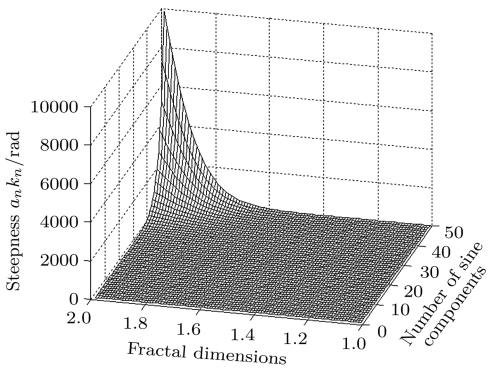


Fig. 6. Variation of fractal dimensions, number of sine components (N) and steepness (s), when $t = 0$ and $x = 10$, where N varies from 1 to 50, and s varies from 1.01 to 2.

The critical value for truncation of fractal parameters can be determined by steepness and energy. One can use Eq. (15) to calculate steepness to find fractal parameters when $\varepsilon_n = 2\pi$. Starting with these initial parameter values, one can find the critical fractal parameters values (for instance, s and N) through Eq. (16):

$$\varepsilon_n^2 - \varepsilon_{n-1}^2 < \tau, \tag{16}$$

where τ is pre-selected to be sufficiently small to ensure that the model does not become ill-posed.

Figure 6 is the result simulated with Eq. (15), those parameters are also basic parameters for the linear model. Thus, our limitations on fractal parameters for the nonlinear model are also applicable to the linear model.

5. Conclusions

Starting from a linear fractal sea surface model in a 1D deep sea, the analytic solution for nonlinear interactions between long and short waves is used to develop a nonlinear fractal sea surface model. Energy conservation and our nonlinear fractal ocean model can explain why spectra intensities of spectra components (whose wavenumbers are $k_n + k_m$ or $k_n - k_m$) should experience change, compared to a corresponding linear fractal model. A method is presented to determine the critical values for fractal parameters, whereby the linear and nonlinear fractal sea surface models avoid being ill-posed.

The nonlinear fractal sea surface is rougher than linear fractal sea surface. Thus, the backscattering radar cross section (RCS) of the nonlinear fractal sea surface model will be different from cases resulting from a linear fractal model. Owing to selected new spectra intensity components appearing in the nonlinear fractal sea surface, with different new wave bands relative to the linear sea surface model, the former represents a potentially more accurate characterisation of the real sea surface. Therefore, nonlinear fractal sea surface model can potentially provide a higher precision backscattering RCS in studies of electromagnetic scattering from the sea surface.

References

[1] Beckmann P and Spizzichino A 1963 *The Scnttering of Electromagnetic Waves from Rough Surface* (New York: Pergamon) p503

[2] Mandelbrot B B 1983 *The Fractal Geometry of Nature* (San Francisco, CA: Freeman) p458

[3] Jakeman E 1982 *J. Opt. Soc. Am.* **72** 1034

[4] Jordan D L, Hollins R C and Jakeman E 1983 *Appl. Phys.* B **31** 179

[5] Jaggard D L and Sun X 1990 *J. Opt. Soc. Am.* A **7** 1131

[6] Berizzi F, Mese E D and Pinelli G 1999 *IEE Proceedings Radar Sonar and Navigation* **146** 55

[7] Berizzi F, Greco M V and Verrazzani L 2000 *IEE Proceedings Radar Sonar and Navigation* **147** 189

[8] Berizzi F and Mese E D 2002 *IEEE Trans. on Antennas and Propagation* **50** 426

[9] Berizzi F, Mese E D and Martorella M 2003 *International Journal of Remote Sensing Taylor and Francis Group* **25** 1265

[10] Martorella M, Berizzi F and Mese E D 2004 *IEEE Trans. Antennas and Propagation* **52** 1193

[11] Xie T, Li B H Chen W J and He Y J 2004 *Proceeding of IGARSS'04* **4** 2772

[12] Xie T, He Y J, Chen W J and Li B H 2005 *Acta Electron. Sin.* **33** 423

[13] Yang J L, Guo L X and Wan J W 2007 *Acta Phys. Sin.* **56** 2106 (in Chinese)

[14] Xie T, Kuang H L, William P, Zou G H, Nan C F, He C, Shen T and Chen W 2009 *Chin. Phys.* B **18** 3090

[15] Ren X C and Guo L X 2008 *Chin. Phys.* B **17** 2491

[16] Longuet-Higgins M S and Stewart R W 1960 *J. Fluid Mech.* **8** 565

[17] He Y J and Alpers W 2003 *J. Geophys. Res.* **108** 3205

[18] Johnson J T, Jakov V T and Brown G S 2001 *IEEE Trans. Geosci. Remote Sensing* **39** 2411

[19] West B J, Brueckner K A and Janda R S 1987 *J. Geophys. Res.* **92** 11803

[20] Donelan M A 1987 *Johns Hopkins APL Technical Digest* **8** 18